Numerical and Experimental Study of Electromagnetic Crimping

R. Kumar*, A. K. Rajak, S. D. Kore

Indian Institute of Technology Guwahati, Assam-781039, India

* Corresponding author: E-mail address: rems2012mt0088@gmail.com; Tel.: +91-7576917872

Abstract

Electromagnetic pulse crimping is a solid state, high speed, and high strain rate joining process. In this process, the flyer is deformed over the base plastically to produce the joint. In this work, copper tube was crimped over the aluminium rod by using single step field-shaper. Finite element analysis, as well as experimental study, was carried out on the single step field-shaper to crimp the copper tube on the aluminium rod. The finite element model was validated based on the measured temperature and outer diameter of the crimped rod. The validated model was used to study the effect of the working length position on the electromagnetic crimping. The variation in the working length position of the field-shaper was analysed to increase the concentration of the electromagnetic pressure at the desired location to produce an effective joint with better mechanical strength. It was found that with the change in the position of the working length of the field-shaper the impact velocity, temperature generation, magnetic field density, and uniformity in crimping of the tube also changes.

Keywords

Electromagnetic crimping, Field-shaper, Joining, Finite element method

1 Introduction

The demand and production of modern light-weight designs require the use of different light weight and high strength materials to fulfill the criteria regarding weight reduction, strength increase, and crash performance. Therefore, not only the development of new materials is required, but it is also of great importance to develop or employ suitable joining techniques.

Electromagnetic crimping (EMC) has a high potential for large-scale industrial production since it is a fast, efficient, and clean process. EMC is a high strain rate, high-speed and solid-state mechanical joining process. This process is popular due to its ability to join the dissimilar materials (Kapil & Sharma, 2015). In EMC process, the components to be joined are known as flyer and base or target. Usually, the flyer is the metal or alloy of higher conductivity such as copper or aluminum, but the base can be of any materials. EMC process is relatively popular in axis-symmetric components such as tube-to-rod, or tube-to-tube joining due to the easy control over the experimental parameters (Haiping, Chunfeng, & Jianghua, 2009).

Yu et al. have studied the application of field shaper in electromagnetic forming and found that the larger the effective area of field shaper results in larger uniform force area and smaller the amount of magnetic pressure Yu et al. have found that magnetic pressure decreases with the increase of the relative diameter of the field shaper (Yu, Li, Zhao, & Li, 2005). Three types of field shaper namely cylindrical, concave and convex were compared by Suzuki et al. for tube bulging and found that the geometry of field shaper and the capacitor energy was the controlling parameter of the amount of the tube bulging. Also revealed that field shaper has a great role in increasing the life of the working coil (Suzuki, Murata, & Negishi, 1987).

A developed electromagnetism module in LS-DYNA for coupled thermal/mechanical/electromagnetic simulations was used for the study. In this module electromagnetic fields for the conductors are solved by using a Finite Element Method (FEM) coupled with a Boundary Element Method (BEM) for the surrounding insulators or air. Both methods FEM and BEM use elements based on discrete differential forms with improved accuracy (Eplattenier & Caldichoury, 2016).
In this work, the EMC process was studied, and the experiments were carried out for manufacturing of copper-aluminum bimetallic rods. The numerical model was validated based on the measured outer diameter of the crimped samples and with the measured temperature. The validated model was used to study the effect of variation in the working length position on the developed temperature and the impact velocity of the tube.

2 Experimental Method and Materials

The electromagnetic crimping of the samples was produced with the tube to rod assembly by using an electromagnetic processing system (EMPS). The MPPS used in this work consist of two capacitors of 45 µF with total discharge energy of 10 kJ. The MPPS transforms the low-voltage power supply 440 V, having 50 Hz frequency into a high-voltage power supply having a range of 0-15 kV, with 16 kHz frequency. The discharge current with peak current 100-150 kA, passes through a multi-turn solenoid coil, which produces an eddy current in the field shaper. In EMC, the produced eddy current provides a Lorentz force that causes the collision of the flyer copper tube onto the fixed inner aluminium rod.

The complete setup of the working zone which consists of the field shaper, solenoid coil, tube and rod is shown in **Figure 1**. The coil used in the process was solenoid coil with 11 number of turn. The diameter of the wire used to manufacture the coil was 4 mm.

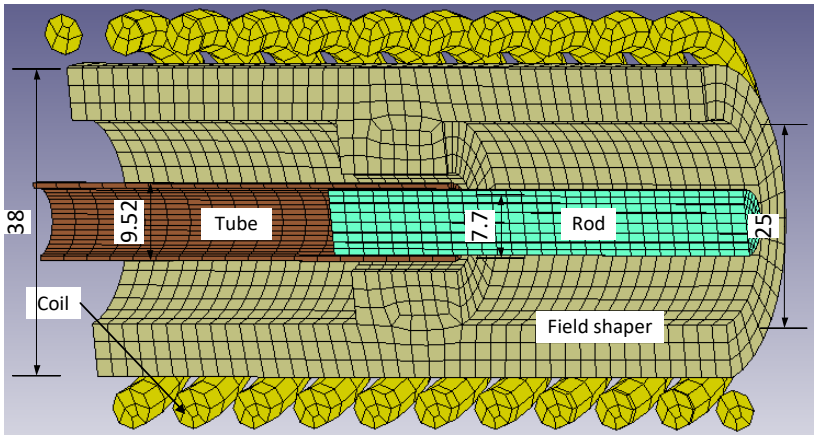

***Figure 1**: EMC process arrangement of tube on rod*

The samples used in the experiments was a copper tube having a thickness of 0.64 mm a flyer tube and aluminum was used as a rigid base material. The detail description of the samples is tabulated in **Table 1**. Copper-Beryllium alloy field shaper was used in the study. The actual image of the field shaper is shown in **Figure 2**. The detail dimensions of the field shaper are shown in **Figure 3**. The outer diameter was 38 mm, and the inner diameter was 12 mm. The length of the working zone was 14 mm.

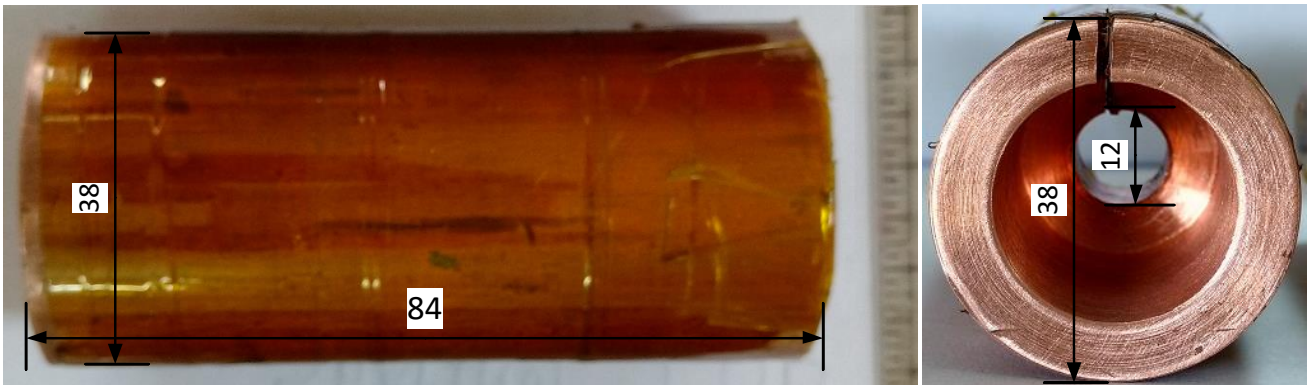

***Figure 2**: Actual image top and front view of the field shaper*

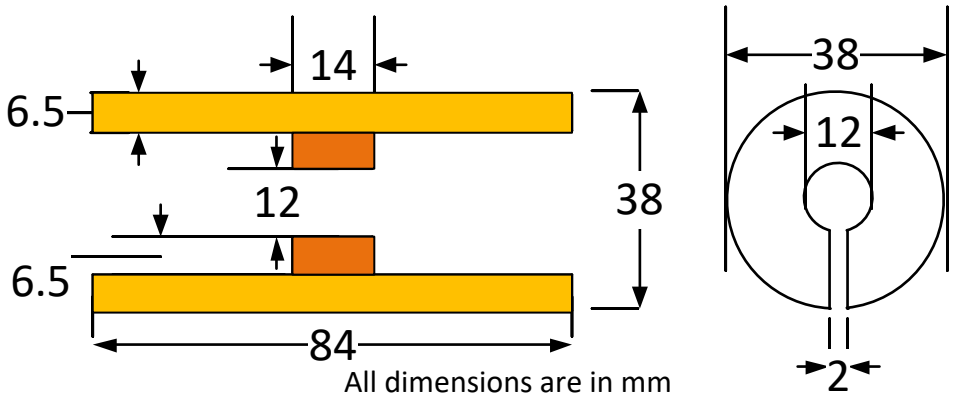

***Figure 3**: Dimensions of the field shaper*

***Table 1**: Measurements and materials of the tube and rod*

Specimen	Materials	Outer diameter	Inner diameter	Length	Thickness	Stand-off
Flyer tube	Copper	9.52 mm	8.24 mm	60 mm	0.64 mm	-
Base rod	Al 1050	7.70 mm	-	60 mm	-	0.27 mm

3 Numerical Details

Electromagnetic crimping is a complex transient high-velocity impact mechanical joining process. It combines different coupling effects of an electromagnetic field, thermal field, and mechanical field. In this study, the electromagnetism module of LS-DYNA was used for coupling the electromagnetic, structural and mechanical process. The source electrical current was introduced into the ends of the solenoid coil to solve the problem related to all together electromagnetic field, structural field, and thermal field.

The Johnson-Cook strain-rate sensitive plasticity model was used for this type of study where the strain rates vary over a large range. In this model, the Johnson-Cook constitutive equation was used to model the behaviour of tubes. The Johnson-Cook equation which is a combination of plastic strain and plastic strain rate can be described by equation (1).

$$\sigma_{eq} = \left(A + B\varepsilon^{n}\right)\left(1 + C\ln\dot{\varepsilon}_{p}\right)\left(1 - \left(\frac{T - T_r}{T_m - T_r}\right)^{m}\right) \quad (1)$$

Where σ_{eq} is flow stress of the material, T_r is the room temperature, T_m is the melting temperature of the material, ε is an equivalent plastic strain, $\dot{\varepsilon}_p$ is plastic strain rate, T is absolute temperature and A, B, C, n, m are Johnson Cook constants (Johnson & Cook, 1983). The values of the Johnson-Cook constants used for copper and aluminum is given in **Table 2**. The values of the mechanical properties of the copper tube and aluminum rod is given in **Table 3**. In a shock compression solid analysis, pressure has to be determined. Therefore, an equation of state is required to define the relationship between volume and pressure in the Johnson-Cook equation. In this study, the linear polynomial equation of state given by equation (2) was used (Vahedi & Khazraiyan, 2004).

$$P = c_o + c_1\mu + c_2\mu^2 + c_3\mu^3 + E_o\,(c_4 + c_5\mu + c_6\mu^2) \quad (2)$$

In equation (2), P is pressure, $c_o, c_1, \ldots, c_6$ are the constant parameters of the linear polynomial equation of state, E_o is the internal energy, and $\mu = \frac{\rho}{\rho_o} - 1$ is compression factor where $\frac{\rho}{\rho_o}$ is the ratio of current density and initial density. The constant coefficients of the linear polynomial equation of state for copper and aluminum are presented in **Table 4** (Vahedi & Khazraiyan, 2004).

***Table 2**: Values of Johnson-Cook material constant parameters*

Materials	A (MPa)	B (MPa)	n	C	T_m (K)	m
Al 1050 (Eide & Melby, 2013)	110	150	0.4	0.01	918	1
Copper (Johnson & Cook, 1985)	92	292	0.31	0.025	1338	1.09

In the simulations, after computing electromagnetic fields by electromagnetic solver at each node the Lorentz force ($\vec{F} = \vec{J} \times \vec{B}$ where J is current density and B is magnetic field density) was evaluated and added to the mechanical solver. In the LS-DYNA thermal solver, the electromagnetic fields also added a Joule heating term which is given by equation (3).

$$Q = \rho J^{2} \quad (3)$$

Where Q is the heat generated per unit volume (in W/m^3), J is the current density (in A/m^2), and ρ is the specific electrical resistivity (in Ω m). The deformation in the tube was obtained by mechanical model which results in new geometry. The temperature generation in the tube was due to tube deformation by high velocity impact and Joule heating. In the simulations, the thermal properties considered were thermal conductivity (k) and the heat capacity (C).

***Table 3**: Material properties of Copper and Al 1050*

Properties	Units	Cu 1010	Al 1050
Density (ρ)	Kg/m^3	8940	2705
Modulus of elasticity (E)	GPa	110	69
Poisson's ratio (v)	-	0.31	0.33
Electrical conductivity (σ)	MS/m	59	37.67
Heat capacity (C)	J/Kg-K	376.8	921
Thermal conductivity (k)	W/m-K	391	231

***Table 4**: Values of linear polynomial equation of state*

Materials	C_o	C_1	C_2	C_3	C_4	C_5	C_6	E_o	V_o
Copper (Maria, 2009)	0	140	2.8	1.96	0.47	0	0	0	1
Aluminum (Schwer, 2009)	0	74.2	60.5	36.5	1.96	0	0	0	1

4 Results and Discussion

The successfully EM crimped samples two of each at five different discharge energy 4.5 kJ, 5.1 kJ, 5.8 kJ, 6.5 kJ, and 7.2 kJ with stepped field shaper is shown in **Figure 4**. In the successfully crimped samples, no wrinkle was observed.

***Figure 4**: EMC process crimped samples*

4.1 Discharge Current Measurement

In the experiments, the discharge current at different energy was measured with the help of Rogowski coil and oscilloscope. **Figure 5** shows the discharged current curve measured during the experiment at five different values of discharge energies. The values of the discharge current used were 4.5 kJ, 5.1 kJ, 5.8 kJ, 6.5 kJ and 7.2 kJ for these energies the peak values of the discharge current were 124 kA, 136.4 kA, 148.8 kA, 161.2 kA and 173.6 kA respectively. The measured discharge current was used as input load in the electromagnetic crimping. Because only the first peak of the discharge current was responsible for high velocity of the flyer tube which results in the deformation followed by joining with the base rod.

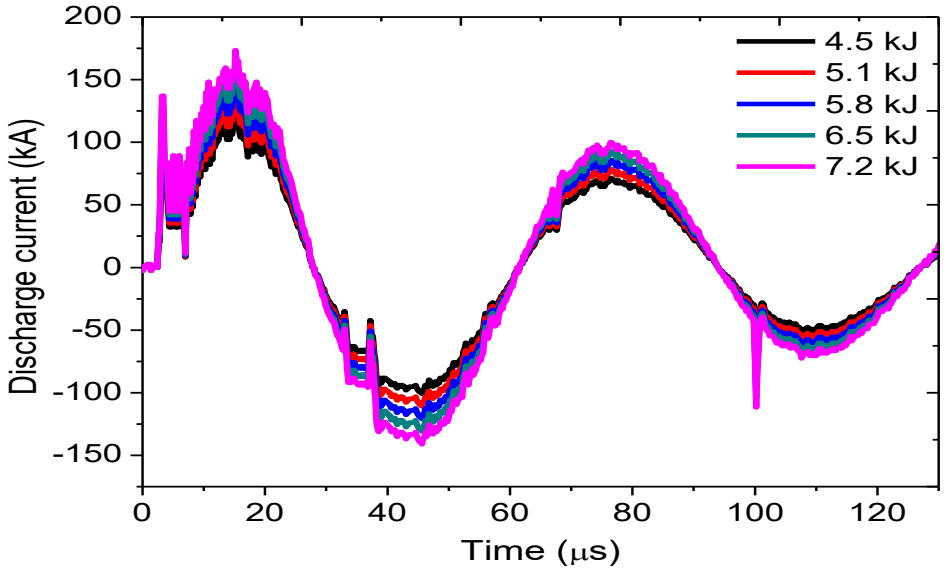

***Figure 5**: Discharge current measured in the experiments*

4.2 Outer diameter measurement

The outer diameter of the successfully crimped sample was measured by using a digital microscope. The outer diameter of the crimped sample obtained from the simulation was also measured in the simulation. The measured outer diameter of the experiment as well as in the simulation is shown in Figure 6. There was a variation in the measured diameter of the crimped samples from the simulated values. A maximum of 6.7 % variation was observed in the simulation data concerning the experimentally measured value. This variation in the values can be due to the large size of the mesh.

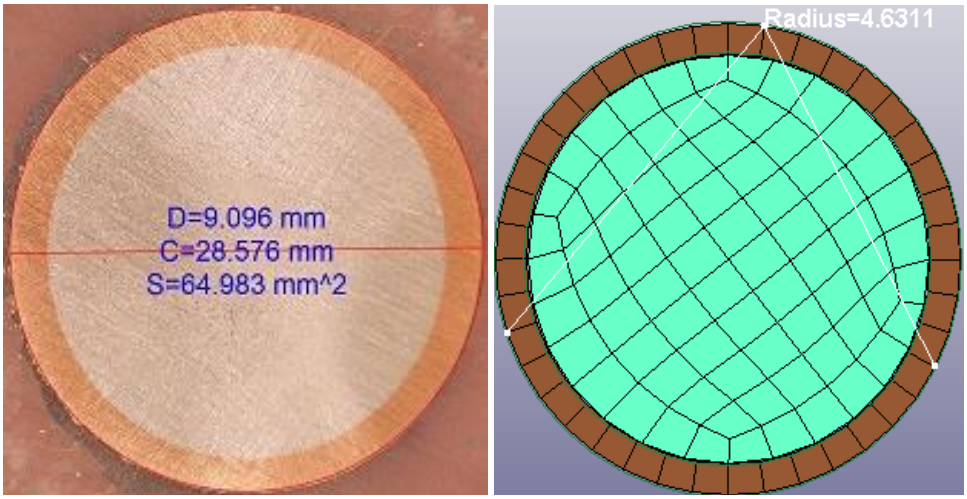

(a) (b)

***Figure 6**: Outer diameter measured in the (a) experiment and (b) simulation*

4.3 Temperature Measurement

The temperature generated in the working zone in the experiment was measured by using infrared (IR) thermometer. The infrared thermometer works on the principle that each body with a temperature above the absolute zero emits electromagnetic radiation from its surface, which is proportional to its intrinsic temperature or infrared radiation.

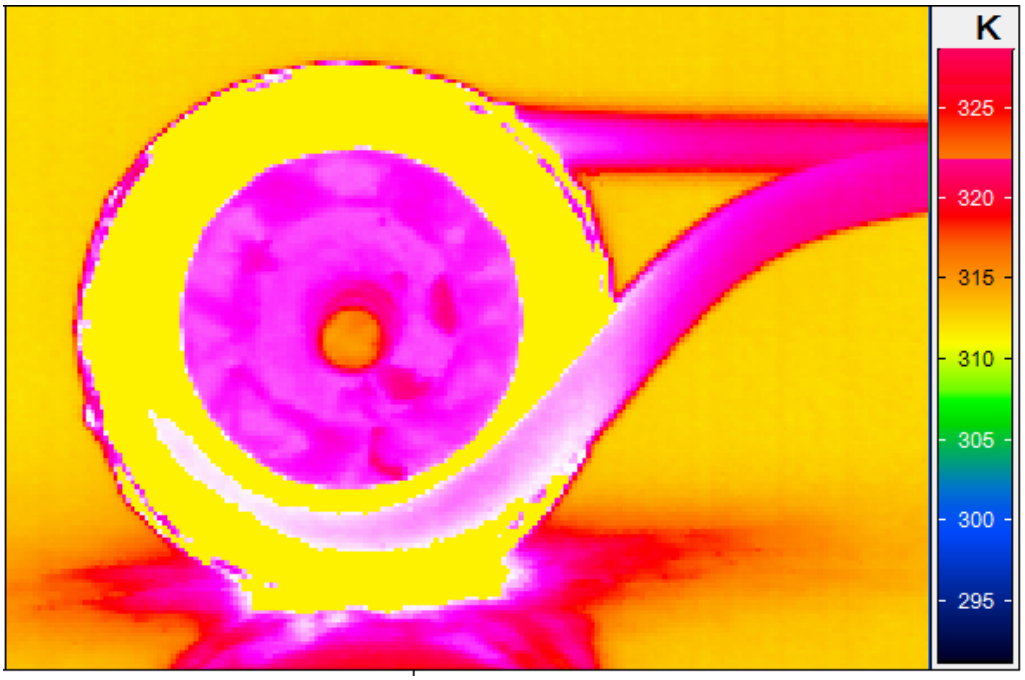

***Figure 7**: Variation in the temperature (in K) in the working zone*

At four different locations, the current was measured. These locations were the points P1, P2, P3, and P4 in the experimental measurement. The similar locations were the elements H72051, H72285, H72357, and H71943 in the simulation model. The same locations can be observed in **Figure 8**. These locations were selected due to visibility while measuring the temperature by the infrared thermometer.

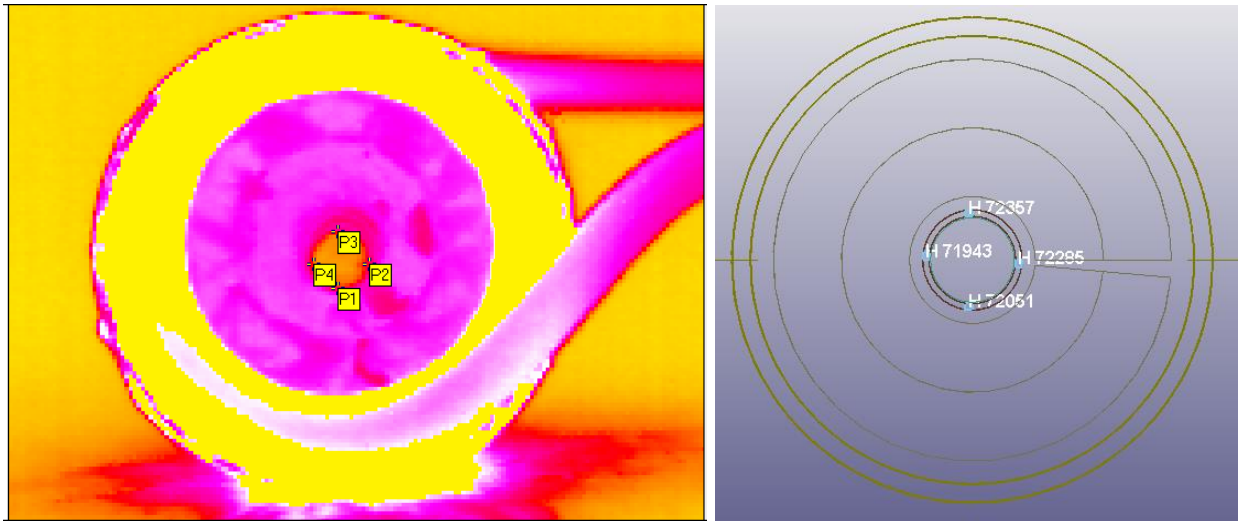

(a) (b)

***Figure 8**: Location of temperature measurement in the (a) experiment and (b) simulation*

The values of the temperature measured at four different locations, both in the experiment as well as in the simulation was plotted. The variation in temperature with peak current (a) experimental and (b) simulated results are shown in **Figure 9**. The temperature changes in the coil and the field shaper was also studied. However, the changes in temperatures in the field shaper as well as in the coil were minimal, and that was below 5 ℃. Hence, the detailed study was not reported for this range of the discharge energy.

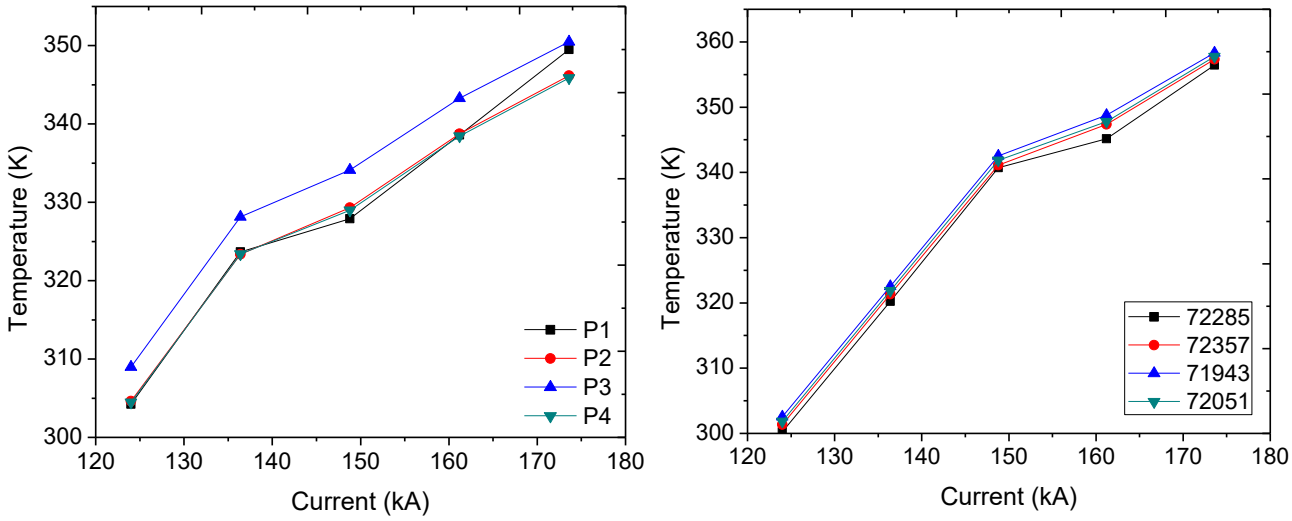

***Figure 9**: Variation in temperature with peak current (a) experimental and (b) simulated results*

The comparative plot of simulated and the experimental values of the maximum temperature with the peak value of the discharge current is shown in Figure 10. It was found that the maximum temperature generated in the simulation was more than that of the experimental values. This variation can be due to leakage of the current and losses in the experiment. The maximum variation in the values of the simulated one was found to be 5.4 %.

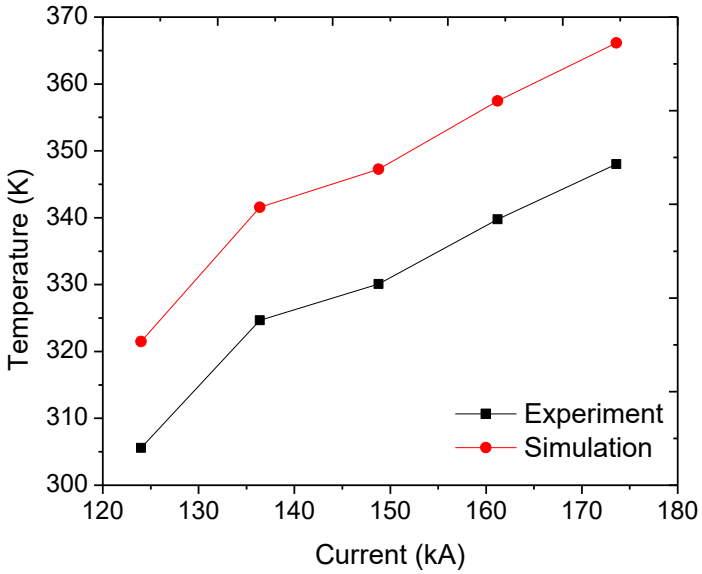

***Figure 10**: Comparison of experimental and simulation results*

4.4 Effect of Working Length Offset

The validated EMC model was used to study the effect of variation in the position of the working length. The position of the working length was varied with 5 mm offset from center in 7 different steps. Seven different field shapes were modeled with the different working length offset. The offset made on the field shaper is shown in **Figure 11**.

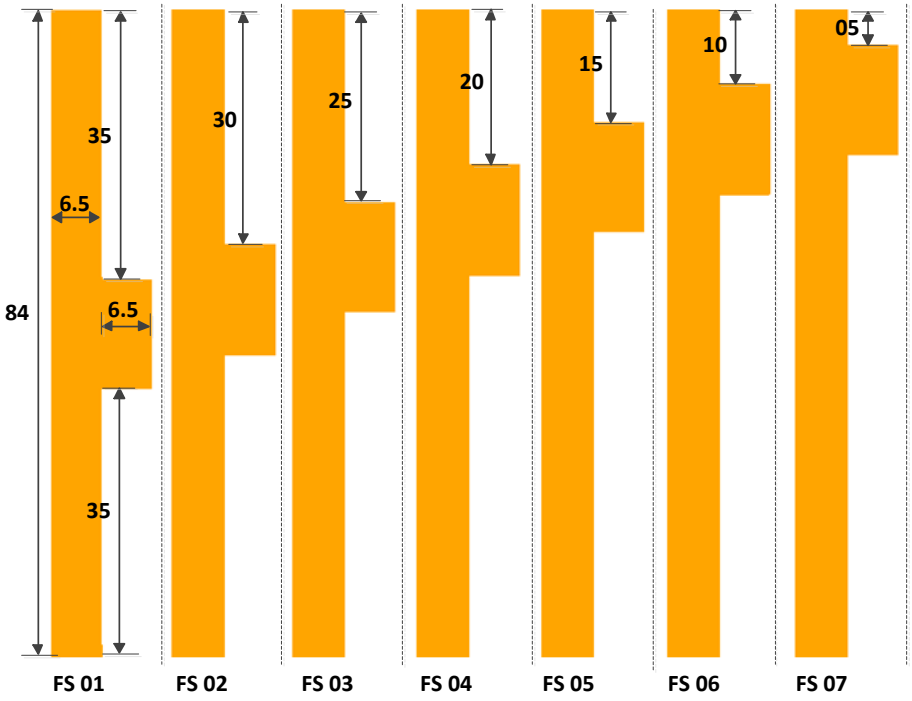

***Figure 11**: Variation in the position of the working length of field shaper*

It was found that with the change in the position of the working length the values of the process parameters also changes. The variation in the impact velocity of the flyer tube with the change in the position of the working length, i.e. working length offset from center is shown in **Figure 12**. The study was completed with three different elements namely H72410, H72427 and H72354 on the circumference of the flyer tube inside the effective or working length.

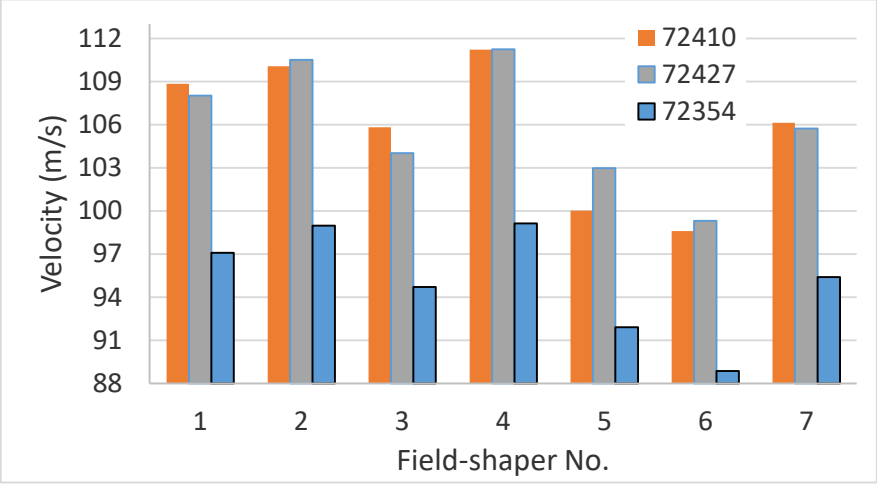

***Figure 12**: Variation in impact velocity with working length position at 7.2 kJ*

The discharge current was also varied with a peak value of 124 kA, 136.4 kA, 148.8 kA, 161.2 kA and 173.6 kA. For all these values of the peak current, the maximum impact velocity was obtained with the 4th field shaper. Also the minimum amount of temperature generated for the same field shaper. The variation in the position of the working length sometimes decreases and sometimes increases the impact velocity, but for all the cases the impact velocity is highest with 4th field shaper. The variation in the temperature generated in the tube with the change in the position of the working length, i.e. working length offset from center is shown in **Figure 13**.

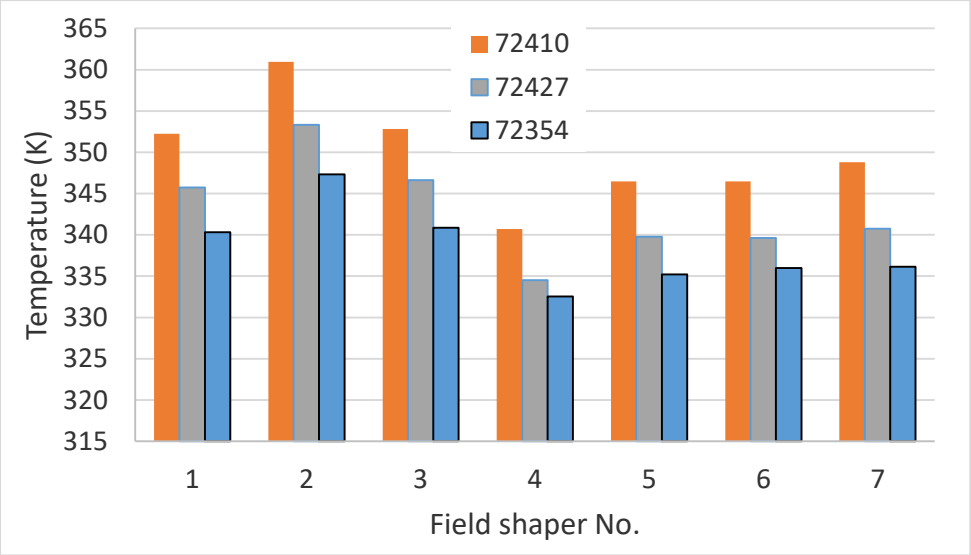

***Figure 13**: Variation in temperature with working length position at 7.2 kJ*

The changes in the magnetic field as well as the change in the current density for developed in these elements namely H72410, H72427, and H72354 were also studied. It was found that with the change in the position of the working length the values of the magnetic field and current density also changes. But in all the cases the values of the magnetic field and the current density found to be minimum. The variation in the magnetic field and the current density with the field shaper is shown in **Figure 14** and **Figure 15** respectively.

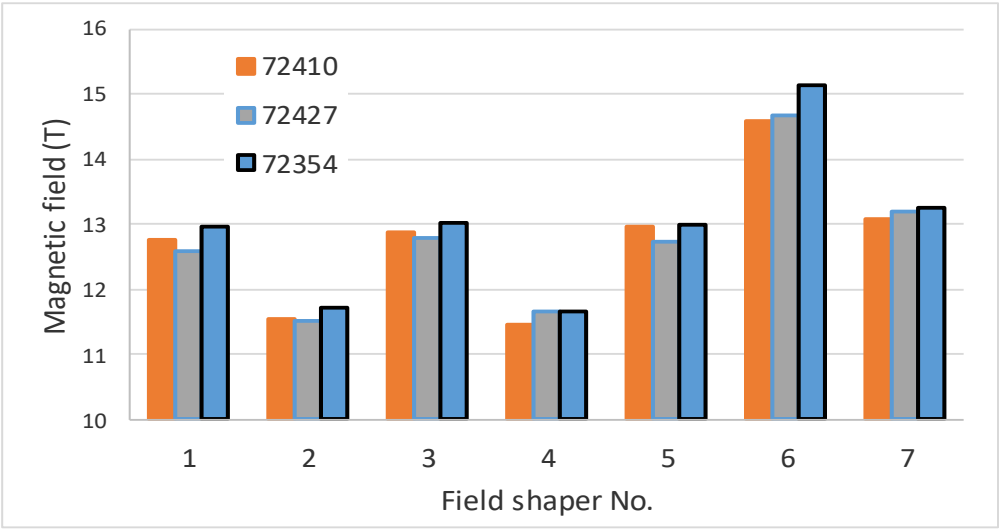

***Figure 14**: Variation in magnetic field with working length position at 7.2 kJ*

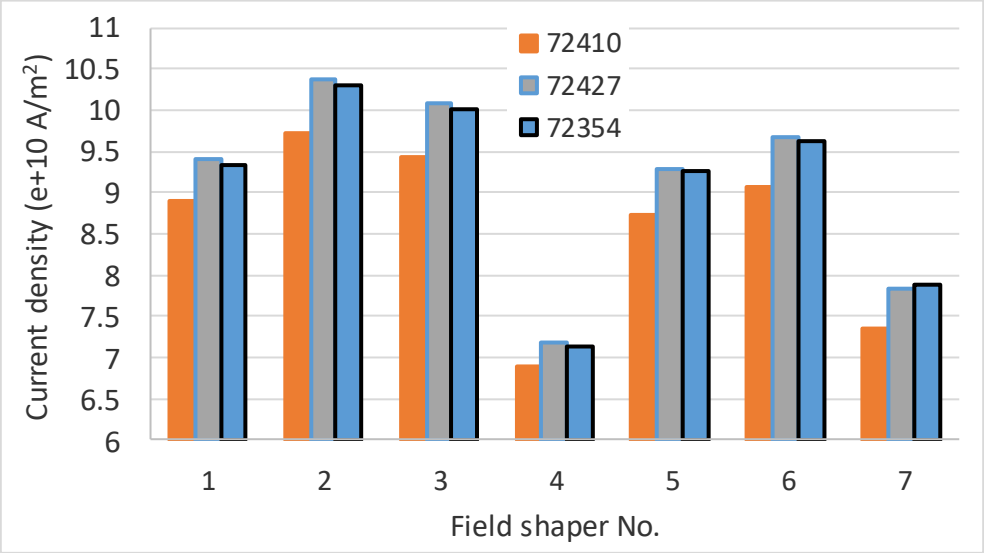

***Figure 15**: Variation in current density with working length position at 7.2 kJ*

The variation in temperature and velocity with 4th field shaper with the peak value of the discharge current for the element H72427 is shown in **Figure 16**. From **Figure 16** it can be concluded that with the increase in the peak current the velocity as well as the temperature generated in the tube increase. This study was completed with the field shaper having 15 mm offset from the center of the field shaper, i.e. by using 4th field shaper. With 4th field shaper, the maximum value of the impact velocity and temperature generated were 111.234 m/s and 334.53 K respectively at 173.6 kA of the discharge current in the element H72427.

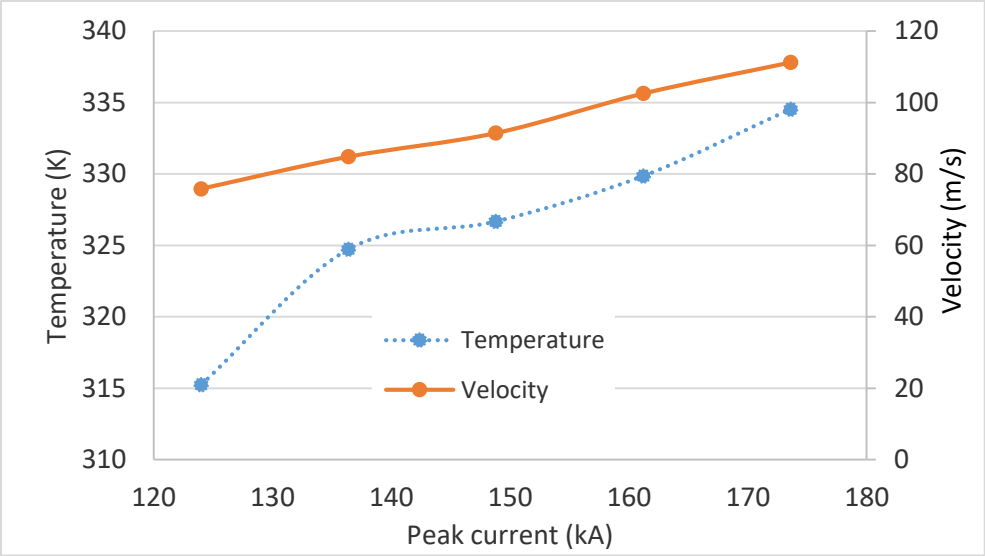

***Figure 16**: Variation in temperature and velocity with 4th field shaper*

The fringe pattern of the impact velocity of the flyer tube with 4th field shaper, i.e. field shaper with 15 mm offset from the center at 7.2 kJ is shown **Figure 17**.

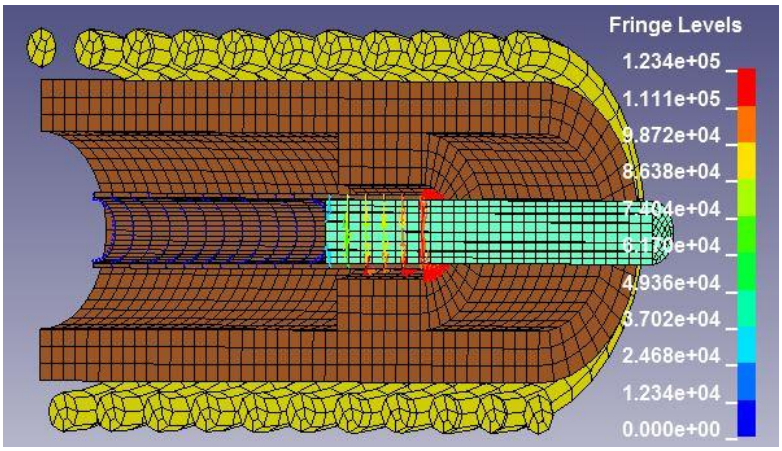

***Figure 17**: Impact velocity of the tube (in mm/s)*

The fringe pattern of the magnetic field at 7.2 kJ of discharge energy is shown in **Figure 18**. The maximum value of the magnetic field density was found to be 11.93 Tesla at 173.6 kA of discharge current with 4th field shaper.

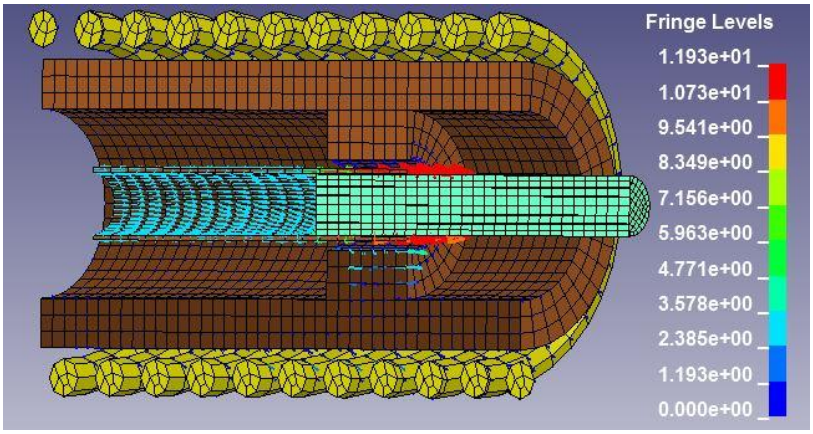

***Figure 18**: Magnetic field induced on the tube (in Tesla)*

The fringe pattern of the current density in the flyer tube with 4th field shaper at 7.2 kJ is shown **Figure 19**. The maximum value of the current density was found to be 5.756 e-4 A/mm^2. At 173.6 kA of discharge current with 4th field shaper.

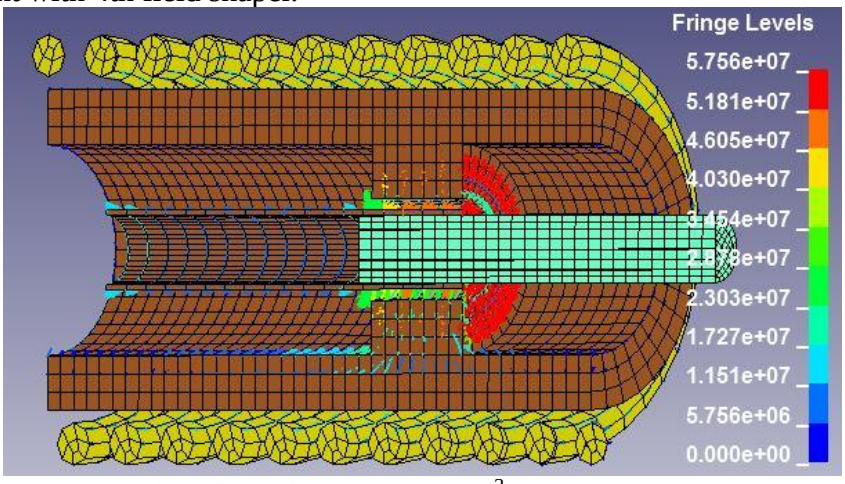

***Figure 19**: Current density induced in tube (in e-3 A/mm^2)*

5. Conclusions

Copper-aluminum combinations of the bimetallic rod/crimped joint were successfully produced by using electromagnetic crimping process. The electromagnetic crimping technique has unique characteristics that it crimps uniformly copper tube on the circumference of the aluminum rod with a complete circular cross-sectional area. The increase in the amount of discharge peak current leads to increase the impact velocity of the tube. The increase in the peak current also leads to decrease in the outer diameter of the crimped rod and increase in the temperature generated in the tube. From this study, it was found that for the 4th type of position i.e. the field shaper having 15 mm offset from the center of the working length gives the highest velocity and lowest temperature generated in the tube. With 4th field shaper, the maximum value of the impact velocity and temperature generated were 111.234 m/s and 334.53 K respectively at 173.6 kA of the discharge current in the element H72427.

References

Eide, H. O., & Melby, E. A. 2013. Blast Loaded Aluminium Plates Experiments and Numerical Simulations. Master Thesis Norwegian University of Science and Technology, 1-139.

Eplattenier, P. L., & Caldichoury, I. 2016. A Coupled 3D/2D Axisymmetric Method for Simulating Magnetic Metal Forming Processes in LS-DYNA. Proceedings of the 7th International Conference on High Speed Forming Dortmund, Germany., 3-12.

Haiping, Y., Chunfeng, L., & Jianghua, D. 2009. Sequential Coupling Simulation for Electromagnetic–Mechanical Tube Compression by Finite Element Analysis. Journal of Materials Processing Technolgy, 209, 707-713.

Johnson, G. R., & Cook, W. H. 1985. Fracture Characteristics of Three Metals Subjected to Various Strains, Strain Rates, Temperatures and Pressures. Engineering Fracture Mechanics, 21(1), 31-48.

Johnson, G., & Cook, W. 1983. A Constitutive Model and Data for Metals Subjected to Large Strain, High Strain Rates and High Temperatures. Proceedings Seventh International Symposium on Ballistic, 541-547.

Kapil, A., & Sharma, A. 2015. Magnetic pulse welding: an Efficient and Environmentally Friendly Multi-Material Joining Technique. Journal of Cleaner Production, 100, 35-58.

Maria, C. 2009. Technology of EHIS (Stamping) Applied to Production of Automotive Parts. Saint-Petersburg State Polytechnical University, Department of Applied Mathematics . Abgerufen am 18. 01 2018 von http://wwwmayr.in.tum.de/konferenzen/Jass09/courses/3/Churilova_paper.pdf

Schwer, L. E. 2009. Aluminium Plate Perforation: A Comparative Case Study using Lagrange with Erosion, Multi-Material ALE, and Smooth Particle Hydrodynamics. 7th European LS-DYNA Conference.

Suzuki, H., Murata, M., & Negishi, H. 1987. The Effect of a Field Shaper in Electromagnetic Tube Bulging. Journal of Mechanical Working Technology, 15, 229-240.

Vahedi, K., & Khazraiyan, N. 2004. Numerical Modeling of Ballistic Penetration of Long Rods into Ceramic/Metal Armors. 8th International LS-DYNA Users Conference, 14, 39-50.

Vedantam, K., Bajaj, D., Brar, N. S., & Hill, S. 2006. Johnson-Cook Strength Models for Mild and DP 590 Steels. American Institute of Physics, 775-779.

Yu, H., Li, C., Zhao, Z., & Li, Z. 2005. Effect of Field Shaper on Magnetic Pressure in Electromagnetic Forming. Journal of Materials Processing Technology, 168, 245-249.

Zhang, P., Kimchi, M., Shao, H., Gould, J. E., & Daehn, G. S. 2004. Analysis of the Electromagnetic Impulse Joining Process with a Field Concentrator. In AIP Conference Proceedings, 712(1), 1253-1258.